Magnetoresistance Effect in Cubic Semiconductors with Spheroidal Energy Surfaces

MOTOICHI SHIBUYA
Electrotechnical Laboratory, Tokyo, Japan

(Received February 26, 1954; revised manuscript received March 30, 1954)

The collision frequency of electrons having a spheroidal energy surface with acoustical modes of vibration is calculated without neglecting phonon energy. Using an asymptotic form in which the collision frequency is proportional to the square root of their energy, the electronic current in a semiconductor in combined magnetic and weak electric fields can be calculated in a closed form by the formal theory of conductivity. The magnetoresistance effect in oriented single crystals of n- and p-type germanium observed by Pearson and Suhl may be discussed consistently at least semiquantitatively with this calculation in both weak and strong magnetic fields.

1. INTRODUCTION

A FRUITFUL study of the magnetoresistance effect in oriented single crystals of germanium was performed by Pearson and Suhl.[1] They compared their results with theories developed by Seitz[2] for weak magnetic fields and by Harding[3] for strong fields, and they found certain discrepancies between the theories and experiment. They pointed out that the theory based upon anisotropies in the relaxation time alone did not agree with their observations and that the idea of nonspherical energy surfaces in the Brillouin zone should be included in a better theory.

It seems, however, that the theory based upon anisotropy in the relaxation time would agree with their observations in p-type samples at least qualitatively, if one took into account the proper sign of the integral I in the electronic theory proposed by Seitz.[4]

There still remain some discrepancies between theory and experiment even when the proper sign of this integral is taken into account. First, Seitz's weak field theory leads to the result that β is negative and both γ and δ are positive, whereas in Pearson and Suhl's experiment δ is negative in the n-type samples; and second, large saturation values of magnetoresistance are observed which cannot be explained with Harding's strong-field calculations.

Johnson and Whitesell[5] have recently studied the effects of both impurity scattering and intrinsic conduction upon the magnetoresistance, and found that the former increases the gap between theory and experiment and the latter decreases the gap. But there are no experimental investigations satisfying the latter condition.

In order to overcome the main discrepancies mentioned above, we here assume cubically equivalent families of spheroidal energy surfaces, the simplest nonspherical form, in the Brillouin zone. First, in the appendix, the collision frequency of electrons having a spheroidal energy surface with acoustical modes of vibration will be calculated along the same lines as in Seitz's theory.[6] The collision frequency of rather high-energy electrons may be proved to be proportional to the square root of their energy; this is the generalization of constant mean free path in the case of a spherical surface. Using this asymptotic form of the collision frequency, in the next section, the current density may be expressed in a closed form as a function of both magnetic and weak electric fields with the same procedure as that used by Blochinzev and Nordheim[7] in discussing the electrical properties of divalent metals. Only three typical but special cases are considered: cubically symmetric families of spheroidal surfaces may be found along six (100) axes (Case a), along twelve (110) axes (Case b), and along eight (111) axes (Case c). In the final section, we show that the observed effects in p- and n-type germanium samples may be semiquantitatively discussed for (Case a) and (Case c), respectively. The validity of the approximations and simplifications in this calculation will be discussed there briefly.

2. THE MAGNETORESISTANCE EFFECT

As shown in the appendix, the asymptotic form of the collision frequency is dependent upon the wave number only through energy. Using this, we can derive the magnetoresistance of a cubic semiconductor in a closed form with the same procedure as that used by Blochinzev and Nordheim[7] who discussed the magnetoresistance in divalent metals.

In the formal theory of conductivity, when the collision frequency depends upon the wave number $\mathbf{K}$ simply through energy and the energy surface is ellipsoidal, the solution of the Boltzmann equation in a weak electric field $\mathbf{E}$ can be obtained in the following finite form without any assumption about the magnitude of the magnetic field $\mathbf{H}$:

$$f=f_0-\phi(df_0/dW), \tag{1}$$

where

$$\phi=(2\pi/h)(\mathbf{G}\cdot\nabla_k W), \tag{2}$$

[1] G. L. Pearson and H. Suhl, Phys. Rev. **83**, 768 (1951).
[2] F. Seitz, Phys. Rev. **79**, 372 (1950).
[3] J. W. Harding, Proc. Roy. Soc. (London) **140**, 205 (1933).
[4] The integral I in Seitz's paper (reference 2) should be negative; Eq. (22c) should read $I=-ne(9\pi\mu^3)/16c^2$.
[5] V. A. Johnson and W. J. Whitesell, Phys. Rev. **89**, 941 (1953).
[6] F. Seitz, Phys. Rev. **73**, 549 (1948).
[7] D. Blochinzev and L. Nordheim, Z. Physik **84**, 168 (1933).

in which

$$\mathbf{G}=\frac{-e\{\nu^2\mathbf{E}-\nu(e/c)[(\mathfrak{M}^{-1}\mathbf{E})\times\mathbf{H}]+(e/c)^2(\mathbf{E}\cdot\mathbf{H})\mathfrak{M}H/\|\mathfrak{M}\|\}}{\nu^2+(e/c)^2(\mathfrak{M}\mathbf{H}\cdot\mathbf{H})/\|\mathfrak{M}\|}, \tag{3}$$

where $\mathfrak{M}$ is the effective mass tensor and $\|\mathfrak{M}\|$ its determinant. Using this distribution function, we can readily calculate the current density $\mathbf{I}$:

$$\mathbf{I}=-(e/2\pi^2h)\int\int\int f\nabla_k W d\mathbf{K}. \tag{4}$$

When the energy surface is given by Eq. (A.1) and the corresponding collision frequency is given by Eq. (A.14), the three components of $\mathbf{I}$ may be expressed in the following closed form, f_0 being Maxwellian:

$$\begin{aligned}
I_1&=NeAr[E_1+\pi^{\frac{1}{2}}B(E_2H_3-E_3H_2)P(X)\\
&\qquad+\{B^2(\mathbf{E}\cdot\mathbf{H})H_1-XE_1\}Q(X)],\\
I_2&=NeA[E_2+\pi^{\frac{1}{2}}B(E_3H_1-rE_1H_3)P(X)\\
&\qquad+\{B^2r(\mathbf{E}\cdot\mathbf{H})H_2-XE_2\}Q(X)],\\
I_3&=NeA[E_3+\pi^{\frac{1}{2}}B(rE_1H_2-E_2H_1)P(X)\\
&\qquad+\{B^2r(\mathbf{E}\cdot\mathbf{H})H_3-XE_3\}Q(X)],
\end{aligned} \tag{5}$$

where N is the carrier density, r and M_1 are given by Eq. (A.5), and three quantities A, B, and X and two functions P and Q are introduced which are defined by the following equations:

$$A=\mu_0 M_1^{-5/2}r^{-2}, \tag{6}$$

$$B=\pm 3\pi^{\frac{1}{2}}A/4c, \tag{7}$$

$$X=B^2\{H_1^2+r(H_2^2+H_3^2)\}, \tag{8}$$

$$P(X)=\{\tfrac{1}{2}-X+\pi^{\frac{1}{2}}X^{\frac{1}{2}}e^X[1-\mathrm{Erf}(X^{\frac{1}{2}})]\}, \tag{9}$$

and

$$Q(X)=1+Xe^X\,\mathrm{Ei}(-X), \tag{10}$$

in which c is the velocity of light and μ_0 is the conductivity mobility in the case of a spherical energy surface, that is, with scalar mass m_0, already obtained by Seitz. Ei is the exponential integral and Erf is the error function integral. In Eq. (7), the plus sign should be taken for hole carriers, and the minus sign for electrons.

To satisfy the cubic symmetry in the Brillouin zone, we must introduce several families of spheroidal surfaces in the case of cubic crystals. Only three special cases are considered in this calculation.

(Case a): We assume that the band edges may occur at six cubically equivalent points $(\pm j, 0, 0)$, $(0, \pm j, 0)$, $(0, 0, \pm j)$, and that at each point we may find a spheroidal energy surface of the same kind, whose rotational axis coincides with each (100) axis, as shown in Fig. 1.

(Case b): In this case, we assume that twelve spheroidal surfaces of the same kind may occur along twelve (110) axes just as in (Case a).

(Case c): In this case, we assume that eight spheroids may occur along eight (111) axes just as in (Case a).

In order to utilize the results obtained above, we assume further that these several families of surfaces are far apart from one another and that the transition of electrons from one family to a different one is forbidden. Thus the total current may be obtained by simply adding the independent currents arising from each family.

In the preceding calculation, for instance in Eq. (5), the coordinate axes defined with suffixes 1, 2, and 3 are so chosen that they form a normal right-hand system in ascending order of suffixes and the 1 axis coincides with the rotational axis of the spheroid. In the following calculation another normal right-hand system with suffixes x, y, and z is introduced, which is formed with the cubic axes (100), (010), and (001) in cubic crystals. The final results will be discussed with this system because of the many advantages which t offers.

(Case a). 6 Spheroids along the (100) Axes

In this case, the component of the total current density parallel to one of the cubic axes may easily be obtained with the following procedure.

The carrier density of each family is $N/6$, and the current density from the $(\bar{1}00)$ family is equivalent to that from the (100) family; and the same relation also holds for the other two pairs. Therefore, permuting the suffixes 1, 2, and 3 in Eq. (5), with x, y, and z, with y, z, and x, and with z, x, and y, successively, summing up the components of current density, and dividing by three, we can obtain the total current density. We will write down only the expression for the x component because the two other components may easily be obtained by changing the suffixes x, y, and z cyclically in this expression:

$$\begin{aligned}
I_x&=(NeA/3)[(r+2)E_x\\
&\quad+\pi^{\frac{1}{2}}B\{E_yH_z[rP(X_x)+rP(X_y)+P(X_z)]\\
&\quad-E_zH_y[rP(X_x)+P(X_y)+rP(X_z)]\}\\
&\quad+rB^2(\mathbf{E}\cdot\mathbf{H})H_x[Q(X_x)+Q(X_y)+Q(X_z)]\\
&\quad-E_x[rX_xQ(X_x)+X_yQ(X_y)+X_zQ(X_z)]],
\end{aligned} \tag{11}$$

where

$$X_x=B^2[H_x^2+r(H_y^2+H_z^2)], \tag{12}$$

and X_y and X_z are obtained by cyclically changing the suffixes x, y, and z in X_x. The two functions P and Q were already defined in Eqs. (9) and (10), respectively.

(Case b). 12 Spheroids along (110) Axes

In this case, the twelve families may be divided into three groups:

x group: (011), $(0\bar{1}\bar{1})$, $(01\bar{1})$, $(0\bar{1}1)$,
y group: (101), $(\bar{1}0\bar{1})$, $(10\bar{1})$, $(\bar{1}01)$,
z group: (110), $(\bar{1}\bar{1}0)$, $(1\bar{1}0)$, $(\bar{1}10)$.

Now the $(0\bar{1}\bar{1})$ family is equivalent to the (011) family as far as the contribution to the total current density is concerned, and the same relation holds also for the other five pairs. Thus the contribution from the x group is obtained when the current density from both the (011) and $(01\bar{1})$ families is given. The cubic components of the current density from the (011) family will be obtained in the following manner. We choose three principal axes of this spheroid for convenience of calculation as follows:

1 axis; (011), 2 axis; $(0\bar{1}1)$, and 3 axis; (100).

The three components of $\mathbf{I}$ along these principal axes, given by Eq. (5) with carrier density $N/12$, can be transformed to the cubic components by

$$I_x=I_3,\quad I_y=2^{-\frac{1}{2}}(I_1-I_2),\quad \text{and}\quad I_z=2^{-\frac{1}{2}}(I_1+I_2). \tag{13}$$

Also, the components of the vectors $\mathbf{E}$ and $\mathbf{H}$ in Eq. (5) may be given as the following linear combinations of cubic components:

$$\begin{aligned}&E_1=2^{-\frac{1}{2}}(E_y+E_z),\quad E_2=2^{-\frac{1}{2}}(-E_y+E_z),\quad E_3=E_x,\\ &H_1=2^{-\frac{1}{2}}(H_y+H_z),\quad H_2=2^{-\frac{1}{2}}(-H_y+H_z),\quad \text{and}\quad H_3=H_x.\end{aligned} \tag{14}$$

As the current density from the $(01\bar{1})$ family can also be obtained with a similar orthogonal transformation, the current density from the x group can readily be calculated. Those from the y and z groups can easily be obtained by cyclically changing the suffixes as usual. Thus the x component of the total current density in this case becomes:

$$\begin{aligned}I_x=&(NeA/3)\big[(r+2)E_x+(B\pi^{\frac{1}{2}}/4)\\ &\times\{(r+1)(E_yH_z-E_zH_y)[P(X_+)+P(X_-)\\ &+P(Y_+)+P(Y_-)+P(Z_+)+P(Z_-)]\\ &+(r-1)[E_yH_z(P(Z_+)+P(Z_-))\\ &-E_zH_y(P(Y_+)+P(Y_-))+(E_yH_y-E_zH_z)\\ &\times(P(X_+)-P(X_-))+E_yH_x(P(Y_+)-P(Y_-))\\ &-E_zH_x(P(Z_+)-P(Z_-))]\}\\ &+(rB^2/2)(\mathbf{E}\cdot\mathbf{H})H_x[Q(X_+)+Q(X_-)\\ &+Q(Y_+)+Q(Y_-)+Q(Z_+)+Q(Z_-)]\\ &-(r+1)(E_x/4)[X_+Q(X_+)+X_-Q(X_-)\\ &+Y_+Q(Y_+)+Y_-Q(Y_-)+Z_+Q(Z_+)+Z_-Q(Z_-)]\\ &+[(r-1)/4]\{E_x[X_+Q(X_+)+X_-Q(X_-)]\\ &+E_y[Z_+Q(Z_+)-Z_-Q(Z_-)]\\ &+E_z[Y_+Q(Y_+)-Y_-Q(Y_-)]\}\big],\end{aligned} \tag{15}$$

where

$$X_\pm=(B^2/2)[(r+1)H^2+(r-1)(H_x^2\pm 2H_yH_z)], \tag{16}$$

and $Y_\pm$ and $Z_\pm$ are given by cyclically changing the suffixes. Also I_y and I_z are obtained with the same procedure.

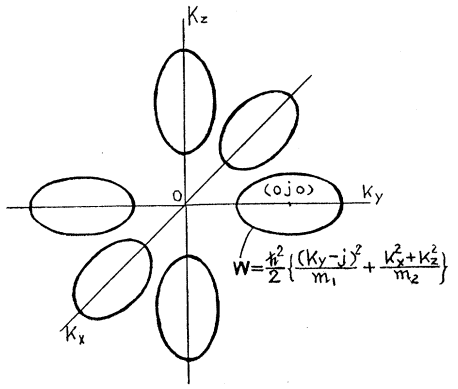

FIG. 1. Schematic diagram of the energy-momentum surfaces in (Case a).

(Case c). 8 Spheroids along (111) Axes

With nearly the same procedure as used in the above two cases, we can obtain I_x in this case as follows,

$$\begin{aligned}I_x=&(NeA/3)\big[(r+2)E_x+(B\pi^{\frac{1}{2}}/4)\\ &\times\{(2r+1)(E_yH_z-E_zH_y)(P_a+P_b+P_c+P_d)\\ &-(r-1)[(E_yH_y-E_zH_z)(P_a+P_b-P_c-P_d)\\ &+H_x((E_y-E_z)(P_a-P_b)+(E_y+E_z)(P_c-P_d))]\}\\ &+(3rB^2/4)(\mathbf{E}\cdot\mathbf{H})H_x(Q_a+Q_b+Q_c+Q_d)\\ &-(r+2)(E_x/4)(X_aQ_a+X_bQ_b+X_cQ_c+X_dQ_d)\\ &-[(r-1)/4][(E_y+E_z)(X_aQ_a-X_bQ_b)\\ &-(E_y-E_z)(X_cQ_c-X_dQ_d)]\big],\end{aligned} \tag{17}$$

where P_i and Q_i $(i=a, b, c, \text{or } d)$ are the abbreviations of $P(X_i)$ and $Q(X_i)$, respectively, and

$$\begin{aligned}X_a=&(B^2/3)[(2r+1)H^2\\ &+2(1-r)(H_yH_z+H_zH_x+H_xH_y)],\\ X_b=&(B^2/3)[(2r+1)H^2\\ &+2(1-r)(H_yH_z-H_zH_x-H_xH_y)],\\ X_c=&(B^2/3)[(2r+1)H^2\\ &+2(1-r)(-H_yH_z+H_zH_x-H_xH_y)],\\ X_d=&(B^2/3)[(2r+1)H^2\\ &+2(1-r)(-H_yH_z-H_zH_x+H_xH_y)].\end{aligned} \tag{18}$$

Now the current density $\mathbf{I}$ in a weak electric field $\mathbf{E}$ may be written in the following matrix form with the conductivity tensor $\mathfrak{L}$,

$$\begin{pmatrix}I_x\\ I_y\\ I_z\end{pmatrix}=\begin{pmatrix}L_{xx}, & L_{xy}, & L_{xz}\\ L_{yx}, & L_{yy}, & L_{yz}\\ L_{zx}, & L_{zy}, & L_{zz}\end{pmatrix}\cdot\begin{pmatrix}E_x\\ E_y\\ E_z\end{pmatrix}. \tag{19}$$

For the three special cases mentioned above, we have already obtained the complicated expressions for this conductivity tensor in a magnetic field. The resistivity tensor $\mathfrak{W}$ can be readily calculated, as it is the inverse tensor of $\mathfrak{L}$. The magnetoresistivity ρ_H will be calculated by the following equation with nine components

TABLE I. Calculated magnetoresistance constants at low magnetic field.

	Case (a)	Case (b)	Case (c)
σ/NeA	$(r+2)/3$	$(r+2)/3$	$(r+2)/3$
$2\alpha/NeAB\pi^{\frac{1}{2}}$	$(2r+1)/3$	$(2r+1)/3$	$(2r+1)/3$
$\beta/NeAB^2$	$-(r^2+r+1)/3$	$-(r+1)^2/4$	$-(r+2)(2r+1)/9$
$\gamma/NeAB^2$	r	$(r^2+4r+1)/6$	$(r+2)(2r+1)/9$
$\delta/NeAB^2$	$(r-1)^2/3$	$-(r-1)^2/12$	$-2(r-1)^2/9$
$-\epsilon'/NeAB^3\pi^{\frac{1}{2}}$	$(2r^2+1)/3$	$(3r^2+2r+1)/6$	$(2r+1)^2/9$
$-\lambda'/NeAB^3\pi^{\frac{1}{2}}$	$r(r+2)/3$	$(7r^2+2r+3)/12$	$(2r^2+1)/3$
$-\eta'/NeAB^3\pi^{\frac{1}{2}}$	$r(r+2)/3$	$(7r^2+2r+3)/12$	$(2r^2+1)/3$

W_{ij} of the resistivity tensor and the direction of the current vector:

$$\rho_H I^2=W_{xx}I_x^2+W_{yy}I_y^2+W_{zz}I_z^2+(W_{xy}+W_{yx})I_xI_y+(W_{yz}+W_{zy})I_yI_z+(W_{zx}+W_{xz})I_zI_z, \quad (20)$$

and the generalized Hall constant R_H in a magnetic field is calculated by

$$R_H=-(\mathbf{E}\cdot[\mathbf{I}\times\mathbf{H}])/(IH)^2. \quad (21)$$

Now we return to our three special cases. Before discussing the magnetoresistivity and generalized Hall constant, some properties of the conductivity tensor are investigated.

The magnetoresistance constants at low magnetic field strength, introduced by Seitz in his equation

$$\mathbf{I}=\sigma\mathbf{E}+\alpha[\mathbf{E}\times\mathbf{H}]+\beta H^2\mathbf{E}+\gamma(\mathbf{E}\cdot\mathbf{H})\mathbf{H}+\delta\mathcal{T}E+\cdots, \quad (22)$$

can readily be obtained with an ascending power series expansion in $\mathbf{H}$ of each component of $\mathfrak{L}$. These are listed in Table I. The normal conductivity and Hall constant are certainly scalar quantities, but they depend differently upon r; thus the relation between the conductivity mobility μ_σ and the Hall mobility μ_H becomes

$$\frac{\mu_H}{\mu_\sigma}=\frac{3\pi}{8}\frac{3(2r+1)}{(r+2)^2}. \quad (23)$$

This relation between the Hall and conductivity mobilities has already been discussed qualitatively with the idea of the re-entrant energy surface by Shockley,[8] but here we consider it quantitatively with spheroids.

There are also some linear relations among the constants which we think are due to the spheroidal approximation. For instance,

$$\beta+\gamma+\delta=0 \quad \text{for Case (a)}, \quad (24)$$

$$\beta+\gamma-\delta=0 \quad \text{for Case (b)}, \quad (25)$$

$$\beta+\gamma=0 \quad \text{for Case (c)}, \quad (26)$$

and

$$\lambda'=\eta' \quad \text{for all of the three cases.} \quad (27)$$

When we put r equal to 1, these small field constants are reduced to those obtained by Seitz in his electronic theory without anisotropy of the relaxation time.

[8] W. Shockley, *Electrons and Holes in Semiconductors* (D. Van Nostrand Company, Inc., New York, 1950).

The magnetoresistivity and Hall constant in a strong magnetic field may be discussed with Eqs. (20) and (21), respectively, but it is in general very tedious. However, it becomes somewhat less laborious when $\mathbf{H}$ is parallel to one of the special crystal axes, for instance, (100), (110), or (111).

When $\mathbf{H}$ is parallel to the (100) axis, the conductivity tensor $\mathfrak{L}$ has the following form, for all three cases:

$$\mathfrak{L}\equiv\begin{bmatrix}L_1, & 0, & 0\\ 0, & L_2, & L_3\\ 0, & -L_3, & L_2\end{bmatrix}. \quad (28)$$

Similarly the resistivity tensor has the same form, and thus the longitudinal magnetoresistivity ρ_{II}, the transverse magnetoresistivity $\rho_\perp$, and the Hall constant R_H become:

$$\rho_{\text{II}}=W_1=1/L_1, \quad \rho_\perp=W_2=L_2/(L_2^2+L_3^2), \quad HR_H=W_3=L_3/(L_2^2+L_3^2). \quad (29)$$

It is very interesting to note that in this case both $\rho_\perp$ and R_H are independent of the vector $\mathbf{I}$.

When $\mathbf{H}$ is parallel to the (111) axis, the resistivity tensor has the following form:

$$\mathfrak{W}\equiv\begin{bmatrix}W_1, & W_2, & W_3\\ W_3, & W_1, & W_2\\ W_2, & W_3, & W_1\end{bmatrix}. \quad (30)$$

Thus ρ_{II}, $\rho_\perp$, and R_H become:

$$\rho_{\text{II}}=W_1+W_2+W_3=(L_1+L_2+L_3)^{-1},$$
$$\rho_\perp=W_1-(W_2+W_3)/2=(2L_1-L_2-L_3)/[(L_1-L_2)^2+(L_2-L_3)^2+(L_3-L_1)^2], \quad (31)$$
$$HR_H3^{-\frac{1}{2}}=(W_2-W_3)/2=(L_2-L_3)/2[(L_1-L_2)^2+(L_2-L_3)^2+(L_3-L_1)^2].$$

When $\mathbf{H}$ is parallel to the (110) axis, $\mathfrak{L}$ has the following form:

$$\mathfrak{L}\equiv\begin{bmatrix}L_1, & L_3, & -L_4\\ L_3, & L_1, & L_4\\ L_4, & -L_4, & L_2\end{bmatrix}, \quad (32)$$

and

$$\rho_{\text{II}}=(W_1+W_3)=(L_1+L_3)^{-1},$$
$$\rho_\perp=(W_1-W_3)-Z^2(W_1-W_2-W_3)=\{L_2+Z^2(L_1-L_2-L_3)\}/\{2L_4^2+L_2(L_1-L_3)\}, \quad (33)$$
$$2^{-\frac{1}{2}}HR=W_4-XZ(W_1-W_2-W_3)=\{L_4+XZ(L_1-L_2-L_3)\}/\{2L_4^2+L_2(L_1-L_3)\},$$

where X and Z are the direction cosines of $\mathbf{I}$ to the (100) and (001) axes, respectively. That is, in this case, the transverse magnetoresistance and the Hall constant depend upon the direction of $\mathbf{I}$.

If we make an asymptotic expansion in $\mathbf{H}$ of the components of the conductivity tensor, the saturation

TABLE II. Calculated saturation magnetoresistance.

H direction	Case (a)	Case (b)	Case (c)
		Saturation values of $\Delta\rho_\infty/\rho_0$ when $\mathbf{I}\parallel\mathbf{H}$	
(100)	0	$(r-1)^2/(5r+1)$	$2(r-1)^2/9r$
(110)	$(r-1)^2/(5r+1)$	$3(r-1)^2/(3r^2+20r+1)$	$(r-1)^2/3(2r+1)$
(111)	$2(r-1)^2/9r$	$(r-1)^2/3(2r+1)$	$2(r-1)^2/3r(2r+7)$
		Saturation values of $9\pi\rho_\infty/32\rho_0$ when $\mathbf{I}\perp\mathbf{H}$[a]	
(100)	$(r+2)(2r+1)/9r$	$(r+2)(3r^2+8r+1)/18r(r+1)$	$(r+2)^2/3(2r+1)$
(111)	$(r+2)^2/3(2r+1)$	$(r^2+4r+1)/6r$	$(r+2)(5r+4)/3(8r+1)$
(110)	$\dfrac{(r+2)[(r+5)+Z^2(r-1)^2/r]}{9(r+1)}$	$\dfrac{(r+2)[(11r+1)(r+1)-Z^2(r-1)^2]}{18r(3r+1)}$	$\dfrac{(r+2)(2r+1)-Z^2(r-1)^2}{9r}$

[a] Z is the direction cosine of $\mathbf{I}$ along the (001) axis.

values of the magnetoresistivity, ρ_∞, and of the Hall constant, R_∞, are easily obtained. To our great surprise, for all of the three cases the saturation Hall constant has the same form

$$R_\infty=(Nec)^{-1}. \tag{34}$$

Thus the same relation as that between drift and Hall mobilities seems to be kept between normal and saturation Hall constants, with the spheroidal approximation, as follows:

$$(R_0/R_\infty)=(\mu_H/\mu_\sigma). \tag{35}$$

Some saturation values of $\Delta\rho_\infty/\rho_0=(\rho_\infty-\rho_0)/\rho_0$ and ρ_∞/ρ_0 are listed in Table II. If one takes $r=1$, these results reduce to those already obtained by Harding, that is, the longitudinal effects disappear and the transverse effects becomes as follows:

$$\Delta\rho_\infty/\rho_0=(32/9\pi)-1=0.132, \tag{36}$$

$$R_0/R_\infty=8/(3\pi)=0.849. \tag{37}$$

Several functions of r listed in Table II are plotted in Fig. 2. One may easily see that in the spheroidal approximation, spherical surfaces give the smallest magnetoresistance effect.

Indeed, all the magnetoresistance effects observed by Pearson and Suhl are at least qualitatively explained with our calculation in this section. In the following section we shall make a semiquantitative discussion and find some quantitative discrepancy between theory and experiment due to the many simplifications and approximations made in this calculation.

3. COMPARISON WITH EXPERIMENT AND DISCUSSION

First, we recalculate the phenomenological magnetoresistance constants β, γ, and δ for small magnetic field, using the experimentally determined values of $\Delta\rho_H/\rho_0H^2$ listed in Table I in the paper by Pearson and Suhl. They determined these constants from the values in the lower three rows of that table, and hence their values are too inaccurate to be used in this discussion; for instance, a magnetoconductive effect would be observed in some cases in p type at 77°K, if they were true. Therefore we use all five rows in that table and determine the average values for the constants. The values thus determined are listed in Table III. One may find there fairly large allowable ranges of average values, which arise from their experiment. This shows that either there were some experimental difficulties or the samples used were not actually cubic.

In Table III, we show also three values of $\beta+\gamma+\delta$, $\beta+\gamma-\delta$, and $\beta+\gamma$ which are used to decide, as a first approximation, with which of those cases considered in the preceding section we may continue to discuss the experimental data semiquantitatively. From this table we can see that Case (a) fits best for p-type samples, and Case (c) fits best for n-type.

(i) p Type

As is seen from Table III, the values of β, γ, and δ satisfy Eq. (24) within the limits of experimental accuracy. Thus we put $\beta+\gamma+\delta$ equal to zero and we use hereafter the following values for β, γ, and δ, respectively: -4.66×10^{-9}, 4.15×10^{-9}, and 0.51×10^{-9}, in the case of p-type germanium at 300°K; and -300×10^{-9}, 273×10^{-9}, and 27×10^{-9} at 77°K, for the following semiquantitative discussion with (Case a).

From the ratio of γ and δ we can determine r, but

TABLE III. Low-field magnetoresistance constants calculated from the experimental data.

	p type		n type	
$10^9\times$	300°K	77°K	300°K	77°K
β	$-4.73\begin{cases}+0.10\\-0.44\end{cases}$	$-300\begin{cases}+14\\-6\end{cases}$	$-0.209\begin{cases}+0.017\\-0.009\end{cases}$	$-66.8\begin{cases}+2.1\\-7.6\end{cases}$
γ	4.08 ± 0.44	274 ± 20	0.187 ± 0.025	57.9 ± 9.7
δ	0.44 ± 0.44	$27\begin{cases}+19\\-22\end{cases}$	$-0.140\begin{cases}+0.029\\-0.022\end{cases}$	$-45.5\begin{cases}+10.1\\-9.4\end{cases}$
$\beta+\gamma+\delta$	$-0.21\begin{cases}+0.98\\-1.32\end{cases}$	$1\begin{cases}+53\\-48\end{cases}$	$-0.162\begin{cases}+0.071\\-0.056\end{cases}$	$-54.4\begin{cases}+21.9\\-26.7\end{cases}$
$\beta+\gamma-\delta$	$-1.09\begin{cases}+0.98\\-1.32\end{cases}$	$-53\begin{cases}+56\\-45\end{cases}$	$0.118\begin{cases}+0.064\\-0.063\end{cases}$	$36.6\begin{cases}+21.3\\-27.4\end{cases}$
$\beta+\gamma$	$-0.65\begin{cases}+0.54\\-0.88\end{cases}$	$-26\begin{cases}+34\\-26\end{cases}$	$-0.022\begin{cases}+0.042\\-0.034\end{cases}$	$-8.9\begin{cases}+11.8\\-17.3\end{cases}$

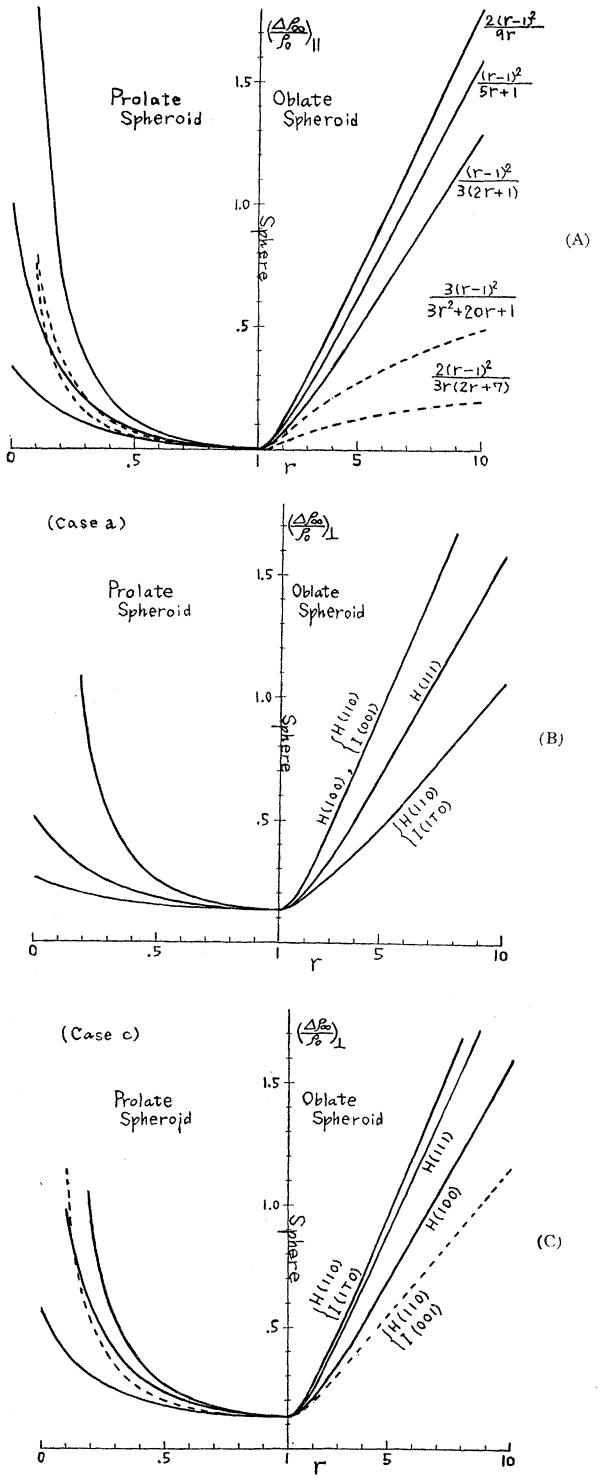

FIG. 2. (A) Saturation values of $\Delta\rho_\infty/\rho_0$ *versus* r, when $\mathbf{H}\|\mathbf{I}$. (B) Saturation values of $\Delta\rho_\infty/\rho_0$ *versus* r, when $\mathbf{H}\perp\mathbf{I}$, in (Case a). (C) Saturation values of $\Delta\rho_\infty/\rho_0$ *versus* r, when $\mathbf{H}\perp\mathbf{I}$, in (Case c).

the equation which determine r is quadratic so we obtain both oblate and prolate solutions. Once r is determined, we can readily obtain the ratio of Hall mobility and drift mobility and also some saturation values of the magnetoresistivity with the formulas in the preceding section. Using the experimental values of the normal conductivity, B will be fixed. With this B value, we can obtain the normal Hall constant R_0, which should be equal to the experimental value, for we already used it in recalculating the magnetoresistance constants. However, unfortunately the discrepancy is large for the case of p-type samples at 300°K. These calculated values are listed in Table IV with the experimental values for comparison. Both the oblate solution and the prolate one explain the observed results to nearly the same extent.

(ii) *n* Type

The data obtained with n-type samples are also treated semiquantitatively with Case (c) in a similar way. The results are listed in Table V. Comparing the calculated values with the experimental ones, we are likely to conclude that the prolate solution fits better for n-type samples.

The experimentally expected saturation values of magnetoresistance in both p- and n-type samples are at least twice as large as the calculated values in this calculation with r, which is determined from the data measured in weak magnetic field. The ratio of the Hall mobility to the drift mobility is given by Eq. (23) in this calculation, but it is about 1.8 for p-type samples at 300°K in the recent experiments at Bell Telephone Laboratories.[9] Closer quantitative agreement between this calculation and those experiments should not be expected at this stage, in consequence of the many simplifications and approximations employed in our calculation.

We may reproduce almost all the curves obtained in Pearson and Suhl's experiment with the appropriate

TABLE IV. Comparison between the calculated values of some magnetoresistance constants in Case (a) and the observed values in p-type Ge.

		300°K			77°K		
Values used in this calculation		σ 2.6 β -4.66×10^{-9} γ 4.15×10^{-9} δ 0.51×10^{-9}			4.6 -300×10^{-9} 273×10^{-9} 27×10^{-9}		
		Calculated		Observed	Calculated		Observed
r		0.55	1.82		0.58	1.72	
$B\times10^5$		4.97	3.33		30.3	21.1	
$R_0\times10^5$		1.4	1.4	0.84	5.1	5.1	4.4
$8\mu_H/3\pi\mu_\sigma$		0.97	0.95	1.5	0.97	0.96	1.0
Directions of H	I		$\Delta\rho_\infty/\rho_0$			$\Delta\rho_\infty/\rho_0$	
(100)	(100)	0	0	~0.1	0	0	~0.1
(110)	(110)	0.054	0.067	~0.1	0.045	0.054	~0.2
(111)	(111)	0.082	0.082		0.068	0.068	
(100)	$I\perp H$	0.23	0.23	~0.5	0.21	0.21	~0.5
(111)	$I\perp H$	0.17	0.19		0.16	0.18	
(110)	(001)	0.23	0.23		0.21	0.21	
(1$\bar{1}$0)	(110)	0.15	0.16	~0.5	0.15	0.16	~0.5

[9] M. B. Prince, Phys. Rev. **92**, 681 (1953); and F. J. Morin, Phys. Rev. **93**, 62 (1954).

values of r and the equations derived in the foregoing section. This is true, for example, of $\Delta\rho_H/\rho_0$ *versus* H, $\Delta\rho_H/\rho_0 H^2$ *versus* H, and $\Delta\rho_H/\rho_0$ *versus* the direction of **H**, but is not true for the finite longitudinal effect along the (100) axis observed in a p-type sample, which cannot be treated with the Case (a). The magnetoresistance effect depends upon temperature only through the generalized mobility A in our calculation. The qualitative agreement between theory and experiment is quite satisfactory. A small part of the quantitative discrepancies between theory and experiment will be corrected in future experiments, but a larger part of them should be corrected in a future, more elaborate, theory. For this reason, we shall restate the simplifications and approximations used in this calculation.

In spite of the complicated energy surfaces in actual crystals, we assume, as one of the simplest nonspherical energy surfaces, spheroids, and we consider only three special cases. It seems rather remarkable that with such a simplification, we have been able to discuss the effects both in n- and p-type germanium semiquantitatively. So we think that the triply degenerate surfaces of complicated form at the top of the valence band may be approximated with three (100) spheroids in the first approximation in connection with the magnetoresistance effect. We also suppose that the bottom of the conduction band may be found nearly along the (111) axis in a future theory of the energy bands of germanium. Herman and Callaway[10] calculated the energy bands in germanium along the (100) axis in the Brillouin zone, and found a shallow minimum along this axis for the conduction bands. Calculations along other axes such as the (110) or the (111) axis are expected, for the magnetoresistance effect in n type cannot be explained with Case (a) but with Case (c) in the present calculation.

We have also assumed that transitions of electrons or holes from a certain family of spheroids to another one are forbidden. This assumption may be quite satisfactory in n type but not in p type. For the normal temperature dependence of electron mobility can be explained with this assumption, but not the anomalous temperature dependence of hole mobility. Of course, this anomaly is due originally to the complicated structure of the top of the valence band; but when we employ the three spheroid approximation mentioned above, it may perhaps be interpreted in terms of the transitions forbidden in this calculation.

The asymptotic form of the collision frequency has been used. This amounts to neglecting the correct behavior of slow electrons, on one hand, but simplifies the calculation a great deal, on the other. The slow electron contribution to the magnetoresistance seems to be very important, however, in many respects. Impurity scattering, which is not considered in this study, is large for slow electrons. Further, even in the case of simple spherical energy surface, using the asymptotic collision frequency (in other words, with the assumption of a constant mean free path), the usual weak magnetic field approximation of expanding the distribution function in ascending powers in H diverges, for this expansion is just the expansion in descending powers of collision frequency which is proportional to the wave number of the electrons. This apparent divergence difficulty can readily be removed by considering the actual collision frequency which is finite for cold electrons whose velocity is smaller than the acoustical velocity. Although we have not encountered such a divergence in this calculation because of the closed form, in spite of using the asymptotic collision frequency which is divergent at $\mathbf{K}=0$, we fear that we may have a little under- or overestimated the magnetoresistance in this calculation by neglecting the actual contribution of slow electrons. One may see the difference between the asymptotic and actual collision frequencies in the figures in the Appendix. The actual collision frequency does not depend simply on **K** only through the energy, so even with the model used in Case (a), the (100) parallel effect seems to be expected, if we can perform the calculation with the actual collision frequency.

As already discussed by Wilson,[11] the fundamental equation used in this study is inadequate for strong magnetic field, but at any rate, qualitative discussions can be made as mentioned above.

Just as was done by Johnson and Whitesell in the case of intrinsic conduction, we can formally combine the results obtained in three cases with appropriate weights, in order to approximate the complicated energy band structure in actual crystals, but it seems meaningless to do this without improving the approximations mentioned above.

TABLE V. Comparison between the calculated values of some magnetoresistance constants in Case (c) and the observed values in n-type Ge.

Values used in this calculation		300°K σ 0.087 β -198×10^{-12} γ 198×10^{-12} δ -140×10^{-12}			77°K 0.59 -64.7×10^{-9} 64.7×10^{-9} -45.5×10^{-9}		
		Calculated	Observed		Calculated	Observed	
r		0.078	12.8		0.079	12.6	
$-B\times10^5$		7.7	1.60		53.3	11.2	
$-R_0\times10^4$		4.4	2.9	4.4	4.5	3.0	4.8
$8\mu_H/3\pi\mu_\sigma$		0.80	0.36	0.87	0.80	0.34	0.86
Directions of **H**	**I**		$\Delta\rho_\infty/\rho_0$			$\Delta\rho_\infty/\rho_0$	
(100)	(100)	2.4	2.4	~4.0	2.4	2.4	~3.0
(110)	(110)	0.25	1.7	~0.5	0.24	1.7	0.5
(111)	(111)	1.01	0.22		1.00	0.22	
(100)	$I\perp H$	0.41	2.1	~1.0	0.41	2.1	~1.0
(111)	$I\perp H$	1.12	2.7		1.11	2.7	
($\bar{1}$10)	(001)	1.50	1.50		1.48	1.48	
($\bar{1}$10)	(110)	2.9	2.9	~6.0	2.8	2.8	~6.0

[10] F. Herman and J. Callaway, Phys. Rev. **89**, 518 (1953).

[11] A. H. Wilson, *The Theory of Metals* (Cambridge University Press, Cambridge, 1936).

We can say in conclusion that the major part of the two main discrepancies between experiment and the previous theories concerning the magnetoresistance effect in cubic semiconductors, mentioned in the first section, is removed. Moreover, the relation between drift and Hall mobilities is discussed, using the simplest nonspherical energy surfaces without introducing any anisotropic relaxation time.

The writer is much indebted to G. M. Hatoyama under whom this research was planned and to W. Sasaki for valuable qualitative discussions. Also he expresses his thanks to Professor F. Seitz, Professor J. Bardeen, and Professor T. Muto who gave him some important comments about the results in Case (a).

APPENDIX (COLLISION FREQUENCY)

The collision frequency of electrons with scalar effective mass in nonpolar crystals has been extensively studied by Seitz. He has pointed out that the acoustical modes of lattice vibration mainly control the collision frequency in actual diamond-type crystals. Therefore, taking only acoustical modes into account, we try here to extend his theory a little further for electrons having spheroidal energy-momentum surface:

$$W=(h^2/8\pi^2)[K_1^2/m_1+(K_2^2+K_3^2)/m_2]. \quad (A.1)$$

If we permit the high-temperature approximation, and assume that the unknown matrix component C would be constant independent of the wave number $\mathbf{K}$, but do not neglect the phonon energy, the collision frequency ν can be obtained as follows:

$$\nu=-(C^2k_0T/9\pi c^2n_0Mh)\Big[\iint_{\substack{A+B\leq 0,\\ 0\leq\theta\leq\pi,\\ 0\leq\varphi\leq 2\pi,}} d\varphi d\theta(\sin\theta)(A+B)D^{-2} + \iint_{\substack{A-B\leq 0,\\ 0\leq\theta\leq\pi,\\ 0\leq\varphi\leq 2\pi,}} d\varphi d\theta(\sin\theta)(A-B)D^{-2}\Big], \quad (A.2)$$

where

$$A=(h^2/2\pi^2)\{(K_1\cos\theta)/m_1+(K_2\cos\varphi+K_3\sin\varphi)(\sin\theta)/m_2\}, \quad (A.3)$$

$$B=hc/2\pi, \quad D=(h^2/8\pi^2)\{(\cos^2\theta)/m_1+(\sin^2\theta)/m_2\},$$

and all other constants have the same meaning as in Seitz's theory. When the phonon term B is neglected and the scalar mass m_0 is used instead of m_1 and m_2, Eq. (A.2) can readily be integrated and gives

$$\nu_0=32\pi^2C^2k_0Tm_0K/9c^2h^3n_0M, \quad (A.4)$$

which was already obtained by Seitz. But now, if one takes into account the effects of the phonon term and the tensor mass in this calculation, the two integrals in Eq. (A.2) have rather complicated ranges of integration and cannot be integrated analytically. In a region near the center of the spheroid, on a $(0,K_2,K_3)$ plane and on a K_1 axis and also in the special case of a spherical energy surface, however, the integration can be done analytically. The collision frequency will be given as a function of the collision frequency ν_0 given by Eq. (A.4), two effective mass ratios M_1 and r which are defined by

$$M_1=m_1/m_0, \quad r=m_2/m_1, \quad (A.5)$$

and four velocity ratios,

$$V_0=2\pi m_0c/hK, \quad V_1=V_0M_1, \quad V_2=V_1r \quad \text{and} \quad V_3=V_1r^{\frac{1}{2}}. \quad (A.6)$$

Case (1): A Spherical Surface

In this case, D becomes independent of the angular variables, so the collision frequency ν_1 of all the electrons in the Brillouin zone can be obtained rigorously, in spite of taking the phonon term B into account:

$$\nu_1=\nu_0\times\begin{cases}2V_0 & \text{for } V_0\geq 1,\\ 1+V_0^2 & \text{for } V_0\leq 1.\end{cases} \quad (A.7)$$

We see in this equation that the collision frequency of rather high-energy electrons can be approximated with the constant mean free path assumption but that of cold electrons is constant independent of the wave number $\mathbf{K}$.

Case (2): $(K_1/m_1)^2+(K_2^2+K_3^2)/m_2^2\leq(2\pi c/h)^2$

In this case, for cold electrons, their velocity is so slow that $A+B$ is always positive; in other words, a phonon-emitting transition is impossible, and $A-B$ is always negative. Thus the range of integration of the

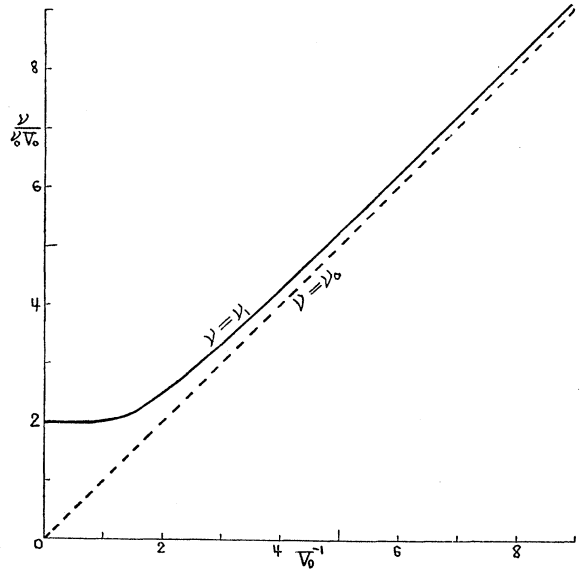

FIG. 3. The collision frequency and its asymptote in the case of spherical energy surface.

second integral corresponding to the phonon-absorbing process becomes very simple. Accordingly the collision frequency ν_2 is readily obtained:

$$\nu_2=\nu_0 M_1 V_2[1+S(r)], \tag{A.8}$$

where

$$S(r)=\begin{cases} r(r-1)^{-\frac{1}{2}}\arctan[(r-1)^{\frac{1}{2}}] & \text{for } r\geq 1, \\ r(1-r)^{-\frac{1}{2}}\operatorname{arctanh}[(1-r)^{\frac{1}{2}}] & \text{for } r\leq 1. \end{cases} \tag{A.9}$$

Thus the collision frequency of cold electrons having a spheroidal energy surface is also finite and constant independent of the wave number **K**.

Case (3): On the K_1 Axis Where $V_1\leq 1$

In this case, although both the phonon-emitting and phonon-absorbing processes are possible, the ranges of integration become independent of an angle variable φ,

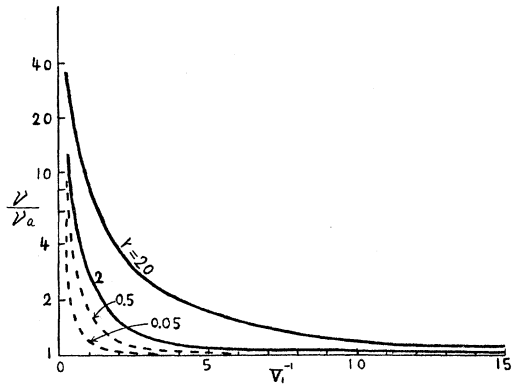

FIG. 4. The ratio of collision frequency and its asymptotic form along the K_1 axis.

and the collision frequency ν_3 can be easily obtained:

$$\nu_3=\nu_0 M_1 r[1+V_1 T(r,V_1)], \tag{A.10}$$

where

$$T(r,V_1)=\begin{cases} r(r-1)^{-\frac{1}{2}}\arctan[V_1(r-1)^{\frac{1}{2}}] & \text{for } r\geq 1, \\ r(1-r)^{-\frac{1}{2}}\operatorname{arctanh}[V_1(1-r)^{\frac{1}{2}}] & \text{for } r\leq 1. \end{cases} \tag{A.11}$$

Case (4): On a $(0,K_2,K_3)$ Plane Where $V_2\leq 1$

In this case, after a certain transformation of integral variables, the ranges of integration become dependent upon only one angle variable just as in Case (3), and the following expression can be easily obtained:

$$\nu_4=\nu_0 M_1 r^{\frac{1}{2}}\{[1+(1-r)V_3^2]^{\frac{1}{2}}+V_3 U(r,V_3)\}, \tag{A.12}$$

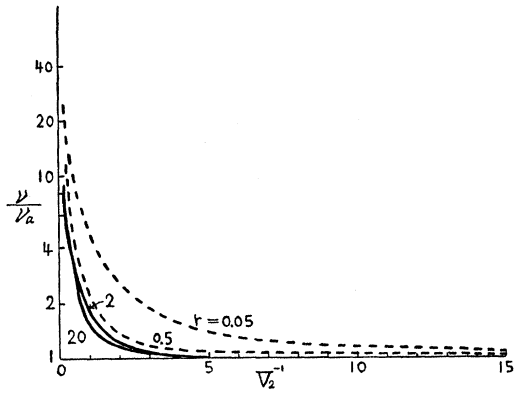

FIG. 5. The ratio of collision frequency and its asymptotic form along the K_2 axis.

where

$$U(r,V_3)=\begin{cases} r(r-1)^{-\frac{1}{2}}\arctan\{V_3(r-1)^{\frac{1}{2}} \\ \quad\times[1+(1-r)V_3^2]^{-\frac{1}{2}}\} & \text{for } r\geq 1, \\ r(1-r)^{-\frac{1}{2}}\operatorname{arctanh}\{V_3(1-r)^{\frac{1}{2}} \\ \quad\times[1+(1-r)V_3^2]^{-\frac{1}{2}}\} & \text{for } r\leq 1. \end{cases} \tag{A.13}$$

From these results rigorously obtained above, we can deduce the asymptotic expression ν_a for the high-energy electrons:

$$\nu_a=\nu_0(m_1m_2^2)^{\frac{1}{2}}(m_0K)^{-1} \times\{K_1^2/m_1+(K_2^2+K_3^2)/m_2\}^{\frac{1}{2}}. \tag{A.14}$$

That is, the collision frequency of rather high-energy electrons is approximately proportional, not to their velocity, but to the square root of their energy.

Indeed it is a very inadequate approximation, for slow or cold electrons, to substitute the actual collision frequency with this asymptotic form, but one may be permitted as a first approximation to use it for all the electrons in the Brillouin zone in the formal theory of electronic conduction, because the calculation then becomes quite simple. Further, the assumption of constant mean free path is used in all the previous theory, and that assumption is also inadequate for slow electrons.

We shall show in the following figures the difference between the actual collision frequency ν and its asymptotic form ν_a. In Fig. 3, ν_1 is plotted as a full line and ν_0, which is the asymptotic form of ν_1, as a dotted line. In Fig. 4, curves of ν/ν_a *versus* **K**, with $r=0.05$, 0.5, 2, and 20, are shown along the K_1 axis, the rotational axis of the spheroid, and in Fig. 5, such curves are shown along any axis perpendicular to the K_1 axis. We can see in these figures that the larger the eccentricity of the spheroid, the less valid is the asymptotic approximation for medium-energy electrons.